Baldwin, J. M (1980) *J. Mol. Biol. 136*, 103-128.
Dlott, D. D., Frauenfelder, H., Langer, P., Roder, H., & DiIorio, E. E. (1983) *Proc. Natl. Acad. Sci. U.S.A. 80*, 6239-6243.
Doster, W., Beece, D., Bowne, S. F., DiIorio, E. E., Eisenstein, L., Frauenfelder, H., Reinisch, L., Shyamsunder, E., Winterhalter, K. H., & Yue, K. T. (1982) *Biochemistry 21*, 4831-4839.
Giacometti, G. M., Brunori, M., Antonini, E., DiIorio, E. E., & Winterhalter, K. H. (1980) *J. Biol. Chem. 255*, 6160-6165.
Gibson, Q. H., Olson, J. S., McKinnie, R. E., & Rohlfs, R. J. (1986) *J. Biol. Chem. 261*, 10228-10239.
Hanson, J. C., & Schoenborn, B. P. (1981) *J. Mol. Biol. 153*, 117-146.
Jajczay, F. L. (1970) Ph.D. Thesis, University of Alberta.
Jongeward, K. A., Magde, D., Taube, D. J., Marsters, J. C., Traylar, T. G., & Sharma, V. S. (1988) *J. Am. Chem. Soc. 110*, 380-387.
Kanaya, E., & Yanagawa, H. (1986) *Biochemistry 25*, 7423-7430.
Kuriyan, J., Wilz, S., Karplus, M., & Petsko, G. A. (1986) *J. Mol. Biol. 192*, 133-154.
Maxwell, J. C., & Caughey, W. S. (1976) *Biochemistry 15*, 388-396.
Mims, M. P., Porras, A. G., Olston, J. S., Noble, R. W., & Peterson, J. A. (1983) *J. Biol. Chem. 258*, 14219-14232.
Morishima, I., Shiro, Y., & Wakino, T. (1985) *J. Am. Chem. Soc. 107*, 1063-1064.
Norvell, J., Nunes, A. C., & Schoenborn, B. P. (1975) *Science (Washington, D.C.) 190*, 568-570.
Ollis, D. L., Appleby, C. A., Colman, P. M., Cutten, A. E., Guss, J. M., Venkatappa, M. P., & Freeman, H. C. (1983) *Aust. J. Chem. 36*, 451-468.
Parkhurst, L. J., Sima, P., & Goss, D. J. (1980) *Biochemistry 19*, 2688-2692.
Phillips, S. E. V. (1980) *J. Mol. Biol. 142*, 531-554.
Phillips, S. E. V., & Schoenborn, B. (1981) *Nature (London) 292*, 81-82.
Rudolph, S. A., Boyle, S. O., Dresden, C. F., & Gill, S. J. (1972) *Biochemistry 11*, 1098-1101.
Shiro, Y., & Morishima, I. (1984) *Biochemistry 23*, 4879-4884.
Stetzkowski, F., Banerjee, R., Marden, M. C., Beece, D. K., Bowne, S. F., Doster, W., Eisenstein, L., Frauenfelder, H., Reinisch, L., Shyamsunder, E., & Jung, C. (1985) *J. Biol. Chem. 260*, 8803-8809.
Szabo, A., & Perutz, M. F. (1976) *Biochemistry 15*, 4427-4428.
Tucker, P. W., Phillips, S. E. V., Perutz, M. F., Houchens, R., & Caughey, W. S. (1978) *Proc. Natl. Acad. Sci. U.S.A. 75*, 1076-1080.
Wittenberg, J. B., Appleby, C. A., & Wittenberg, B. A. (1972) *J. Biol. Chem. 247*, 527-531.

Crystal Structure of the Carbon Monoxide–Substrate–Cytochrome P-450$_{CAM}$ Ternary Complex[†,‡]

Reetta Raag and Thomas L. Poulos*

Center for Advanced Research in Biotechnology of the Maryland Biotechnology Institute, University of Maryland, Shady Grove, 9600 Gudelsky Drive, Rockville, Maryland 20850

Received March 9, 1989; Revised Manuscript Received May 3, 1989

ABSTRACT: The crystal structure of the ternary complex formed between carbon monoxide (CO), camphor, and ferrous cytochrome P-450$_{CAM}$ has been refined to an *R* value of 17.9% at 1.9-Å resolution. To accommodate the CO molecule, the substrate, camphor, moves about 0.8 Å while at the same time remaining in nonbonded contact with CO. The average temperature factor of the camphor atoms is about 50% higher in the CO complex, suggesting that the camphor is more loosely bound in this ternary complex. The Fe–C–O angle is about 166°, and thus, CO appears to be bent from the heme normal, as it is in various CO–globin complexes, due to steric interactions with active site groups. The oxygen atom of the CO molecule is nestled into a groove formed by an unusual helical hydrogen bond in the distal helix between the highly conserved Thr 252 and Gly 248 residues. In the transition from the ferric camphor-bound binary complex to the ferrous CO–camphor-bound ternary complex, the heme iron atom moves into the plane defined by the pyrrole nitrogens by about 0.41 Å. Although the axial Cys ligand also moves toward the heme, the S–Fe bond stretches from about 2.20 Å in the absence of CO to about 2.41 Å once CO has bound.

Cytochromes P-450 are a group of *b*-type heme proteins that catalyze the hydroxylation of aromatic and aliphatic substrates in a variety of metabolic processes. The most extensively studied P-450 is the camphor hydroxylase from *Pseudomonas putida*, or P-450$_{CAM}$ (Wagner & Gunsalus, 1982; Gunsalus et al., 1974; Debrunner et al., 1978; Gunsalus & Sligar, 1978). P-450$_{CAM}$ is a 45 000-dalton polypeptide containing a single ferric protoporphyrin IX. This enzyme converts camphor to 5-*exo*-hydroxycamphor as the first step in the oxidative assimilation of camphor as a carbon source.

The most characteristic feature of all P-450s is the unusual 450-nm Soret band of the ferrous CO complex which is considerably red shifted relative to that of most other ferrous CO

[†] Supported in part by NIH Grant GM 33688.
[‡] The atomic coordinates of the CO–camphor–P-450$_{CAM}$ structure have been deposited in the Brookhaven Protein Data Bank.
* To whom correspondence should be addressed.

0006-2960/89/0428-7586$01.50/0

heme proteins (Garfinkel, 1958; Klingenberg, 1958). In contrast, the oxy-P-450 spectrum closely resembles those of oxyglobins [Dawson and Eble (1986) and references cited therein]. The unusual 450-nm band of the CO complex has been attributed to the proximal Cys heme ligand in P-450; globins and peroxidases contain an axial His ligand (Stern & Peisach, 1974; Collman & Sorrell, 1975; Chang & Dolphin, 1975, 1976). A more detailed analysis of the CO complex attributes the 450-nm band to a charge-transfer interaction between the anionic mercaptide Cys ligand and the heme (Debrunner et al., 1978; Hanson et al., 1976).

In addition to the spectroscopic and electronic differences of CO- and O_2-heme protein complexes, these complexes are also somewhat different geometrically. In structurally unhindered model heme complexes, CO binds along the normal to the porphyrin plane, forming a linear group with the Fe atom (Peng & Ibers, 1976). The Fe–O–O group, in contrast, is bent in model heme complexes (Collman et al., 1974). However, when bound to hemoglobin, CO and O_2 are found to lie off of the heme normal, apparently due to steric interactions with surrounding protein groups (Baldwin, 1980; Shaanan, 1983). In contrast to the Fe–O–O group which is considerably nonlinear, it is believed that the Fe–C–O group tends to remain linear even when displaced from the heme normal; thus, the Fe–C–O group is "tilted" more than "bent" (Collman et al., 1976; Peng & Ibers, 1976) although in model heme complexes in which the CO binding site is quite crowded the Fe–C–O unit is able to bend (Busch et al., 1981).

On the basis of the ferric camphor–P-450$_{CAM}$ crystal structure, we had previously modeled a diatomic ligand to the heme iron and found that a linear Fe–ligand bond was unlikely as a result of crowding in the active site (Poulos et al., 1987). Moreover, there appears to be insufficient room for both the substrate, camphor, and a CO or O_2 molecule unless the substrate moves in the ternary complex. Finally, we have postulated that a distortion and widening of the groove between Gly 248 and Thr 252 in the distal helix provides a binding site for O_2 that is conserved in all P-450s (Poulos et al., 1987). Eventually, we hope to determine the crystal structure of the O_2–camphor–P-450$_{CAM}$ ternary complex to test directly our hypotheses. However, stabilization of this complex will require cryogenic techniques, which we are currently implementing in our laboratory. In the meantime, we have chosen to investigate the considerably more stable CO–camphor–P-450$_{CAM}$ complex as a model for the O_2–camphor–P-450$_{CAM}$ complex. On the basis of the similarities between the CO- and O_2–hemoglobin structures mentioned above (Baldwin, 1980; Shaanan, 1983), and since CO and O_2 are both diatomic molecules, we believe that such a comparison is warranted and may yield further insight into the mechanism of action of the P-450 enzymes.

Materials and Methods

P-450$_{CAM}$ was crystallized according to our earlier procedure (Poulos et al., 1982). Crystals first were converted to the camphor-bound complex by soaking in an artificial mother liquor consisting of 40% saturated ammonium sulfate, 0.05 M potassium phosphate, and 0.25 M KCl adjusted to pH 7.0 and saturated with camphor. CO gas was bubbled through 10 mL of the same mother liquor for several minutes prior to the addition of 174 mg of dithionite to give approximately 0.1 M dithionite. While bubbling with CO was continued, the pH was adjusted to 7 with 5 N KOH. Crystals then were soaked in the dithionite–CO mixture under CO gas for about 1 h. After the crystal was mounted in an X-ray capillary, the capillary was flushed with CO and sealed with CO-saturated mother liquor followed by a plug of mineral oil.

Table I: Summary of Data Collection

maximum resolution (Å)	1.90
total observations	73 981
R_{sym}[a]	0.072
% data collected to	
3.44 Å	97
2.73 Å	89
2.39 Å	77
2.17 Å	70
2.01 Å	66
1.90 Å	43
$I/\sigma(I)$ at	
2.17 Å	3.05
2.01 Å	1.72
1.90 Å	0.97

[a] $R_{sym} = \sum|I_i - \langle I_i\rangle|/\sum I_i$, where I_i = intensity of the ith observation and $\langle I_i\rangle$ = mean intensity.

Table II: Summary of Crystallographic Refinement

resolution range (Å)	10.0–1.9
refections measured	24 228
reflections used, $I > 2\sigma(I)$	18 785
number of atoms/asu[a]	3534
number of solvent atoms/asu	238
number of variable occupancy factors/asu	240
R factor[b]	0.179
rms deviation of bond distances (Å)	0.018
rms deviation of bond angles (Å)	0.030
rms deviation of dihedral angles (Å)	0.033

[a] asu, asymmetric unit. [b] $R = \sum|F_o - F_c|/\sum F_o$.

To ensure that the above treatment leads to the formation of the expected CO adduct and not conversion to the inactive form of the enzyme known as P-420 (Yu & Gunsalus, 1974), the following control experiment was carried out. Several crystals too small for X-ray studies were converted to the CO–camphor–P-450$_{CAM}$ ternary complex as described above. These crystals were dissolved in a dithionite-free, CO-saturated buffer consisting of 0.05 M potassium phosphate, 0.25 M KCl, and 0.8 mM camphor, and the visible absorption spectrum was recorded. The characteristic 446-nm band of P-450 was present. There was no indication of P-420.

X-ray intensity data were collected from a single crystal on a Nicolet area detector with a Rigaku rotating anode. Data were relatively complete to about 2.2 Å, as can be seen from Table I.

Crystallographic refinement was carried out with the restrained parameters–least-squares package of programs (Hendrickson & Konnert, 1980). Briefly, initial $2F_o - F_c$[1] and $F_o - F_c$ difference Fourier maps were based on structure factor calculations using coordinates from the refined camphor–P-450$_{CAM}$ structure (Poulos et al., 1987) and diffraction data obtained from the CO–camphor–P-450$_{CAM}$ complex. Camphor coordinates were omitted from the initial phase calculation. $F_o - F_c$ maps were contoured at $\pm 3\sigma$ and $2F_o - F_c$ maps were contoured at $+0.5\sigma$ and $+1\sigma$ (σ is the standard deviation calculated over an entire asymmetric unit of the difference electron density map). The final refined $2F_o - F_c$ difference map is shown in the top panel of Figure 1, and a summary of the refinement is provided in Table II.

Both $2F_o - F_c$ and $F_o - F_c$ difference electron density maps showed the presence of a sixth ligand, presumably a CO molecule, bound to the iron atom. In addition, difference maps

[1] Abbreviations: EXAFS, extended X-ray absorption fine structure spectroscopy; F_o, observed structure factors; F_c, calculated structure factors; PCN, 16α-cyanopregnenolone; rms, root mean square.

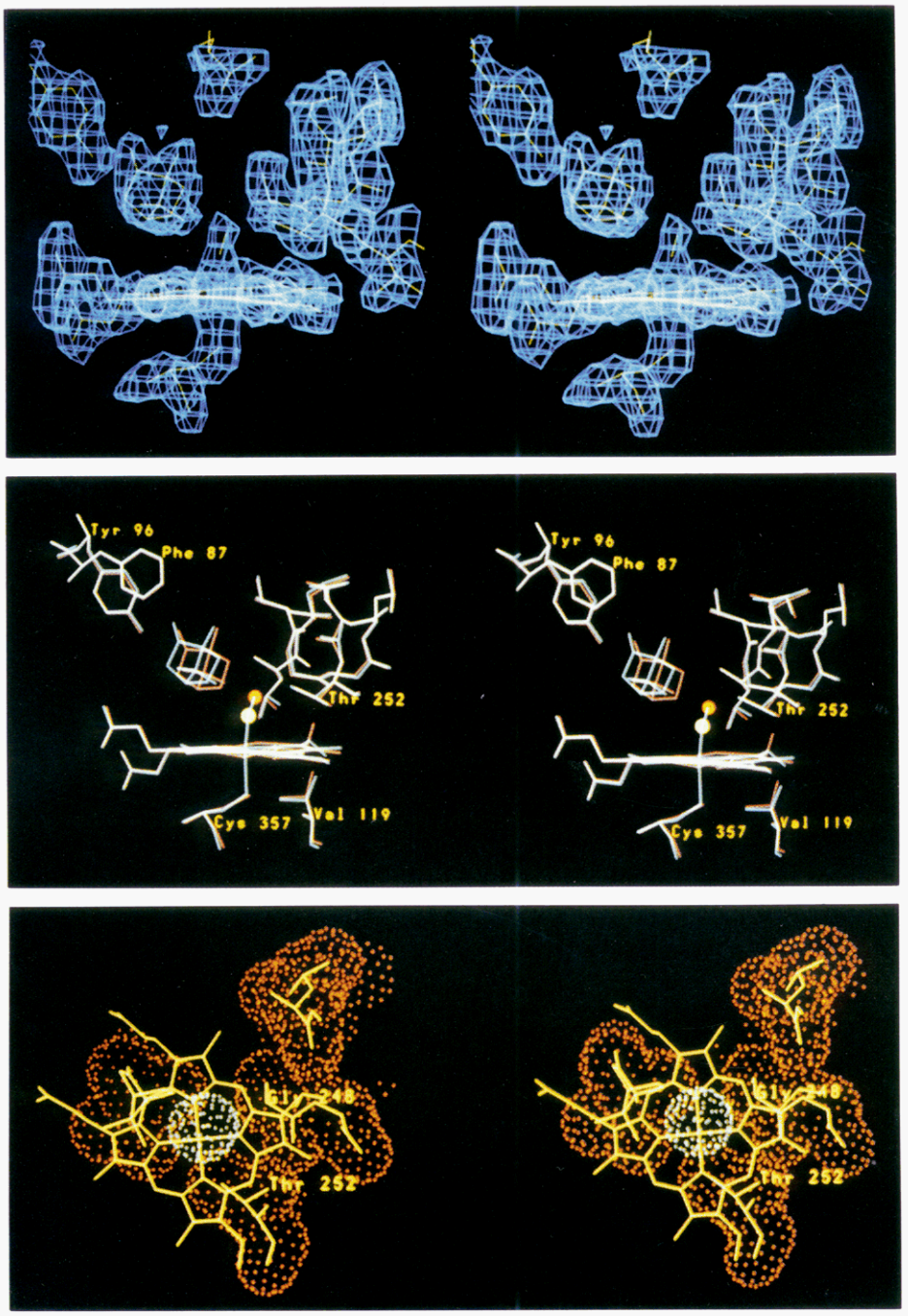

FIGURE 1: (Top) Stereoscopic view of final $2F_o - F_c$ map, contoured at $+1\sigma$, with final refined (restrained) coordinates of the CO–camphor–P-450$_{CAM}$ complex superimposed. Although camphor and CO coordinates were included in the phase calculation for this map, the map calculated from phases generated from a model without camphor and CO is virtually identical with the one shown. (Middle) Stereoscopic view of refined coordinates of the CO–camphor–P-450$_{CAM}$ complex (blue) superimposed on the refined coordinates of the camphor–P-450$_{CAM}$ complex (red). Note the CO molecule bent from the heme normal in the CO–camphor–P-450$_{CAM}$ complex toward the distal helix and the heme vinyl group which has flipped, resulting in movement of Val 119. (Bottom) van der Waals surfaces of CO ligand (blue), distal helix (red, right side of CO), and camphor (red, left side of CO). CO forms nonbonded contacts with both camphor and the distal helix, primarily with Thr 252 and Gly 248. Note that the distal helix, CO, and camphor are all on the same (distal) side of the heme plane and are shown here projecting toward the viewer.

indicated that the camphor molecule should be repositioned *away* from the CO molecule and heme and toward Phe 87. However, even when contoured at 0.5σ, the density of the oxygen atom of CO was rather weak, possibly indicating that the CO ligand either has some freedom to precess about the heme normal, that it can adopt a number of discrete conformations, or that it is not bound at full occupancy. Refinement was continued with both the CO and camphor molecules included in the model, both initially with full occupancy.

It also was not clear whether to include the CO ligand in the refinement as covalently bound to the heme iron atom or as a free molecule. Thus, both approaches were taken. When the CO molecule was considered covalently attached to the heme, the Fe–C bond length was restrained toward 1.8 Å [Baldwin, 1980; p 959 of Wells (1986)]. In both cases the C–O bond length was restrained toward 1.15 Å [Steigemann & Weber, 1979; p 959 of Wells (1986)]. With CO included as part of the heme, nonbonded contacts between the CO carbon atom and pyrrole nitrogen atoms forced the Fe–C bond to lie along the heme normal. Following refinement against such a model, $F_o - F_c$ maps clearly indicated that the CO group should be tilted away from the heme normal. Furthermore,

Table III: Comparison between EXAFS, Model Heme Complexes, and the Present Study of Various Bond Distances in the Ferric Camphor–P-450$_{CAM}$ and Ferrous CO–Camphor–P-450$_{CAM}$ Complexes[a]

plane	S–Fe^{3+}	S–Fe^{2+}, CO complex	Fe^{2+}–C, CO complex	Fe to pyrrole N plane, Fe^{3+} pentacoordinate	Fe to pyrrole N, Fe^{2+} CO complex
protein, X-ray	2.20 (2.19)	2.41 (2.35, 2.36)	2.04 (1.76, 1.61)	0.43 (0.44)	0.02 (0.02, 0.09)
EXAFS	2.24[b]	2.34[b]	1.72[b]		
model hemes, X-ray	2.32[c]	2.352[d]	1.78[d]	0.43[c]	0.02[d]

[a] All distances are in angstroms, and those in parentheses are from unrestrained refinements. [b] Hahn et al. (1982). [c] Koch et al. (1975). [d] Caron et al. (1979).

camphor and CO refined to a closest approach distance of 2.2 Å, an unacceptably short distance. Thus, we chose not to include CO as part of the heme during subsequent refinement. Furthermore, modeling of CO–heme adducts as two independent groups is not without precedent (Steigemann & Weber, 1979).

Once the restrained CO–camphor–P-450$_{CAM}$ model had refined to our satisfaction, albeit with a bent Fe–C–O group (see below), several final refinement cycles were carried out during which all temperature factors of CO, camphor, and solvent atoms and occupancies of CO and solvent atoms alternately were allowed to refine. Temperature factors did not change much. Temperature factors for the CO carbon and oxygen atoms increased from 20.8 and 23.3 Å^2 to 21.2 and 23.4 Å^2, respectively. However, the occupancy of the carbon atom of CO remained at 1.00, whereas that of the oxygen atom dropped to 0.88. While it is not physically reasonable for atoms of the same molecule to have different occupancies, these results indicate that the oxygen atom of CO is indeed more mobile or disordered than the carbon atom.

With the CO and heme modeled as two separate groups, van der Waals contacts between the CO carbon atom and heme iron atom tended to push the CO farther from the heme than it really was, as suggested by the Fe–C distances found for model heme complexes (Peng & Ibers, 1976; Busch et al., 1981). To clarify the stereochemistry of the Fe–C–O linkage in P-450$_{CAM}$, refinement was carried out without restraints on bond distances, angles, or nonbonded contacts. Following such unrestrained refinement, the Fe–C distance was considerably shorter than it was in the restrained model (Table III). Refinement of the heme and CO as two groups also resulted in another problem: the Fe–C–O angle did not remain linear. As mentioned in the introduction, transition metal–carbonyl complexes are expected to be linear (Peng & Ibers, 1976). Thus, a different kind of unrestrained refinement was carried out. To keep the Fe–C–O complex linear as well as to allow it to tilt away from the heme normal, the Fe–C–O unit was modeled as a single group and the porphyrin without iron as a separate group.

Results and Discussion

In the middle panel of Figure 1, the refined ferrous CO–camphor ternary complex is shown superimposed on the ferric camphor-bound binary complex (Poulos et al., 1985, 1987). In Table III we list relevant bond distances.

Refinement and Errors. A major problem for crystallographic analyses at less than atomic resolution is the assignment of errors to distances such as those listed in Table III. In order to help estimate such errors, the least-squares refinement was repeated with no restraints on bond angles, distances, and nonbonded contacts. Differences between atomic positions as determined by restrained and by unrestrained refinements provide simple error estimates of atomic positions. Distances obtained from unrestrained refinements are listed in parentheses in Table III.

Interestingly enough, atoms did not always refine to the same positions when unrestrained refinements were carried out from slightly different initial conditions. For example, the Fe–S distance was set from its value of 2.41 Å (the result of the restrained refinement) to 2.30 Å either by torsionally rotating the sulfur atom of the axial Cys ligand or by moving the Fe atom toward the proximal ligand. No other changes were made in the model. Following identical unrestrained refinements, both Fe–S distances converged to about 2.35 Å. However, as a result of the first unrestrained refinement, the Fe–C and C–O bond lengths had become 1.76 and 1.24 Å, respectively, whereas the second unrestrained refinement had changed these values to 1.61 and 1.40 Å, respectively. Moreover, the Fe–C–O angles refined to 157° and 168° in the two different unrestrained refinements. In both cases of unrestrained refinement, the CO ligand approached more closely to the Fe atom than it did following restrained refinement.

On the basis of the rms difference in the position of the CO molecule in the restrained and unrestrained refinements, we estimate that the error in positioning the CO molecule is about 0.11 Å. Therefore, much of the variation in the Fe–C bond length is due to inaccuracy in locating the CO molecule and not the iron atom, the position of which did not vary greatly as a result of unrestrained refinement.

CO Ligand Geometry. Despite this uncertainty in CO position, the CO ligand always refined to a position off of the heme normal, tilted away from the camphor molecule, and directed toward the distal helix near Thr 252. Such an orientation of the CO molecule was confirmed by electron-density maps based on both restrained and unrestrained models and "unbiased" electron-density maps where the model used for the structure factor calculation did not contain the CO molecule. Furthermore, as mentioned under Materials and Methods, when the CO ligand was constrained to be perpendicular to the heme plane, $F_o - F_c$ difference electron-density maps contoured at $\pm 3\sigma$ indicated that the ligand should be tilted away from the heme normal. Finally, when the iron atom and CO molecule were modeled as a single unit with a linear Fe–C–O angle and the porphyrin as another unit, unrestrained refinements not only tilted the CO off of the heme normal but gave a Fe–C–O bond angle of about 171°. Taken together, these results suggest that steric constraints force the CO molecule both to bend and to tilt away from the heme normal.

In myoglobin (Norvell et al., 1975) and hemoglobin (Heidner et al., 1976; Steigemann & Weber, 1979), the Fe–C–O unit also is bent from the heme normal, with an Fe–C–O angle of about 135° in myoglobin. Similar bending was expected in camphor-bound P-450 on the basis of infrared (O'Keefe et al., 1978) and resonance Raman studies (Uno et al., 1985). In the present study the Fe–C–O bond angle is much closer to being linear, about 166°, suggesting that the steric restraints in forming a nearly linear Fe–C–O bond are less severe in

P-450 than they are in the globins. In P-450$_{CAM}$ the substrate provides the primary steric constraint while in the globins the distal His ligand and neighboring Val and Phe residues crowd the O_2-binding pocket.

Changes in Heme Geometry. Beyond the presence of the CO ligand located off of the heme normal, there are two significant differences between the camphor–P-450$_{CAM}$ and the CO–camphor–P-450$_{CAM}$ structures. One difference is in the position of the iron with respect to the porphyrin core and associated changes in heme geometry, and the second is in the positions of the camphor molecule and various protein groups. First, we consider changes in the heme and iron–ligand distances. In the ferric camphor-bound state the iron atom is displaced from the heme porphyrin core toward the proximal Cys ligand by about 0.43 Å, but in the ferrous CO complex this displacement is only 0.02 Å in the restrained model and 0.02–0.09 Å in the unrestrained models. Thus, upon reduction and binding of CO, the heme iron atom moves into the plane defined by the pyrrole nitrogens of the heme by about 0.41 Å. The data in Table III also show that the S–Fe bond stretches from 2.20 to 2.41 Å (restrained model) in the ferric camphor to ferrous CO–camphor transition.

The crystallographically determined S–Fe bond lengths of 2.20 and 2.35–2.41 Å for the ferric camphor–P-450$_{CAM}$ and ferrous CO–camphor–P-450$_{CAM}$ complexes, respectively, are to be compared with bond lengths of 2.24 Å (ferric) and 2.33 Å (ferrous CO), as determined by EXAFS studies (Hahn et al., 1982; Kau et al., 1986). The S–Fe distance is 2.352 Å in the crystalline model thiolate–heme–CO complex, $[C_2H_5$-SFeTTP(CO)]$^-$ (Caron et al., 1979). EXAFS studies on model heme complexes also indicate that, with a neutral thiol rather than an anionic thiolate ligand, the S–Fe bond length is 2.40 Å or greater (Kau et al., 1986). Regarding the question of Cys ligand protonation, iterative extended Hückel calculations (Hanson et al., 1976) support the experimental findings with model systems (Collman & Sorell, 1975; Stern & Peisach, 1974) that a neutral thiol ligand would generate a band near 420 nm while an anionic thiolate ligand would give the 450-nm band characteristic of P-450. Judging by the long S–Fe bond (2.41 Å) in our restrained model, we were concerned that we may have generated the inactive P-420 species with a thiol rather than a thiolate ligand to iron. However, as noted under Materials and Methods, the spectrum of the CO–camphor–P-450$_{CAM}$ crystals dissolved in buffer gave the 446-nm band expected for P-450. Moreover, single-crystal polarization spectra of P-450$_{CAM}$ orthorhombic I crystals also exhibit the 446-nm band (Debrunner et al., 1978). Although orthorhombic I crystals belong to a different space group ($P2_12_12$) than those we are currently using ($P2_12_12_1$), both crystal types are prepared under similar conditions from ammonium sulfate. Taken together, these data indicate that the crystalline CO–camphor–P-450$_{CAM}$ complex prepared for this study is P-450 and not P-420. The difference between the S–Fe bond distance found in the EXAFS and the present study (about 0.02–0.08 Å) is attributable to experimental error and not to fundamental differences in the electronic properties of the species used to obtain the data.

One final change in heme geometry is rotation of one of the heme vinyl groups by about 140° such that it points "up" in the ferric camphor complex and "down" in the ferrous CO–camphor complex (Figure 1, middle panel). This rotation may be the result of changes in the electronic properties of the heme following reduction and/or CO binding rather than a strictly conformational effect of CO binding, since the overall movement of the distal helix, which would apparently be involved in this "push" of the vinyl, appears to be too small to initiate such a rotation. One conformational consequence of the vinyl group rotation is that Val 119, and to a smaller extent helix C in which it is located, must move away from the heme to make room for the vinyl group in its new position.

Changes in the Substrate. In order to avoid unfavorable contacts with the CO molecule, camphor in the CO–camphor–P-450$_{CAM}$ complex must move *away* from the CO molecule by about 0.8 Å (Figure 1, middle panel). The need to avoid clashing with camphor also appears to be the primary reason why the CO molecule does not lie along the heme normal in this complex. Despite movement of the substrate, the camphor carbonyl oxygen–Tyr 96 OH hydrogen bond remains intact, and the camphor forms nonbonded contacts with the CO molecule. Furthermore, the average temperature factor for camphor atoms increases from 16.2 to 24.8 Å^2 in the transition from the ferric camphor–P-450$_{CAM}$ binary complex to the ferrous CO–camphor–P-450$_{CAM}$ ternary complex, indicating that the camphor is not as firmly held in place in the CO complex. In addition, the temperature factors of protein atoms in the region around Thr 185 are slightly higher in the CO-bound than in the CO-free structure. This region is part of the postulated substrate access channel (Poulos et al., 1986) and is also slightly expanded in the CO-bound structure. The sensitivity of the Thr 185 region of P-450$_{CAM}$ to changes in the active site is further evidenced by increases in thermal parameters in this region in the substrate-free enzyme (Poulos et al., 1986) and in complexes formed with various inhibitors of P-450$_{CAM}$ (Poulos & Howard, 1987). The binding of CO by camphor–P-450$_{CAM}$ thus appears to involve a compromise between optimal enzyme–substrate interactions and the preference of CO to form a linear complex with the iron atom. The CO molecule, which has its highest affinity when bound along the heme normal (Collman et al., 1976), is forced to bend away from its optimal position by the substrate while at the same time camphor–protein interactions decrease somewhat to allow CO to bind.

Changes in the Protein. In the bottom panel of Figure 1 are shown van der Waals contacts between CO, camphor, and protein in the restrained structure. The camphor molecule forces the CO molecule toward the distal helix where the CO oxygen atom fits into an opening in this helix formed by a hydrogen bond between the peptide carbonyl oxygen atom of Gly 248 and the side-chain hydroxyl group of Thr 252. This Gly 248–Thr 252 hydrogen bond disrupts the normal helical hydrogen-bonding pattern in the distal helix and generates a groove slightly larger than those found in helixes with "normal" hydrogen-bonding patterns. Moreover, due to slight movements in the side chain of Thr 252 and the backbone of Gly 248, this opening is somewhat larger in the presence than in the absence of CO. As we have argued elsewhere (Poulos et al., 1987), we suspect that this helical distortion is a structural feature found in all P-450s and is important in forming the O_2 binding site. With the exception of rat liver P-450$_{PCN}$, Thr 252 is conserved in all P-450s for which sequence data are available (Nelson & Strobel, 1988). Rat liver P-450$_{PCN}$, however, contains a Pro instead of a Thr, which is expected to cause the same local disruption in the helix.

Mechanistic Implications. Movement of camphor upon binding of CO may have relevance to the catalytic mechanism. We expect that the O_2–camphor–P-450$_{CAM}$ complex will be very similar to the CO–camphor–P-450$_{CAM}$ complex just described. However, once the dioxygen bond is cleaved, following reduction by a second electron to leave a single iron-linked activated oxygen atom (presumably the hydrogen-abstracting

species), the camphor molecule probably returns at least part of the way toward the position it occupies in the binary ferric camphor–P-450$_{CAM}$ complex. Hydrogen-abstraction and oxygen-addition steps would then follow.

A puzzling problem in understanding the hydroxylation of camphor is how to reconcile the observed lack of stereospecificity in abstraction of the C5 hydrogen atom of camphor with the strict stereospecificity in forming the 5-*exo*-hydroxy product. Although 5-exo abstraction is preferred, Gelb et al. (1982) have found that both 5-exo and 5-endo hydrogen atoms can be removed while only the 5-exo product is formed. From the estimated positions of the two camphor C5 hydrogen atoms, it appears that the 5-exo hydrogen is about 1.5 Å closer than the 5-endo hydrogen atom to the carbon atom of CO, the putative location of the iron-linked oxygen atom presumed responsible for hydrogen abstraction. The camphor 5-carbon atom, the camphor 5-exo hydrogen atom, and the carbon atom of CO are also virtually collinear. Moreover, the camphor 5-carbon atom, the camphor 5-exo hydrogen atom, and the presumed location of an activated oxygen lone-pair orbital are collinear, providing almost ideal geometry for hydrogen abstraction. In contrast, the camphor 5-endo hydrogen atom points away from the CO molecule to form about a 60° angle between the camphor 5-carbon atom, the camphor 5-endo hydrogen atom, and the activated oxygen atom location. We believe these observations explain the observed preference toward 5-exo hydrogen abstraction and hydroxylation (Gelb et al., 1982).

Our present study demonstrates that camphor mobility increases in the CO complex, and presumably, similar substrate mobility characterizes the O_2–camphor–P-450$_{CAM}$ complex. Thus the fact that 5-endo hydrogen abstraction is found at all may be because the mobility of camphor could allow occasional presentation of the 5-endo hydrogen atom to the hydrogen-abstracting species. However, if mobility is the reason that the 5-endo hydrogen atom is occasionally removed, one might also expect some 5-endo-hydroxylated product, yet only the 5-exo product is found (Gelb et al., 1982). We would expect a camphor radical from which a hydrogen had been abstracted to be as mobile in the active site, if not more so, as the camphor molecule. Hence, mobility may be more of a factor in influencing the hydrogen-abstraction step than it is in the actual hydroxylation step. It would thus appear that if the iron-linked oxygen atom is involved in both hydrogen-abstraction and oxygen-addition steps (Groves et al., 1978), the latter process, addition of the OH$^{\bullet}$ radical to the substrate radical, may have the more strict geometrical requirements. The importance of substrate mobility in influencing the products of the P-450 reaction is further supported by the findings that the substrate norcamphor is metabolized to at least three hydroxylated products by P-450$_{CAM}$ (Atkins & Sligar, 1988) and that from the X-ray structure determination of the norcamphor–P-450$_{CAM}$ complex norcamphor was found to have significantly higher mobility in the active site than does camphor (Raag & Poulos, 1989).

Although our results are consistent with the widely held view that a single iron-linked oxo intermediate operates as the catalytically important species in both the hydrogen-abstraction and oxygen-addition steps and that variations in stereospecificity of the two steps are controlled by substrate mobility, there is at least one alternate mechanism. One must also consider a model in which the "hydrogen-abstracting and oxygen-adding species are separate and distinct entities" (Gelb et al., 1982). Candidates for these species include an oxygen radical which would be released after homolytic fission of the O–O bond or the less likely prospect of a protein-centered radical.

ACKNOWLEDGMENTS

We thank Evon Winborne for assisting with the color photographs.

REFERENCES

Atkins, W. H., & Sligar, S. G. (1988) *Biochemistry 27*, 1610–1616.

Baldwin, J. M. (1980) *J. Mol. Biol. 136*, 103–128.

Busch, D. H., Zimmer, L. L., Grzybowski, J. J., Olszanski, D. J., Jackels, S. C., Callahan, R. C., & Christoph, G. G. (1981) *Proc. Natl. Acad. Sci. U.S.A. 78*, 5919–5923.

Caron, C., Mitschler, A., Rivere, G., Ricard, L., Schappacher, M., & Weiss, R. (1979) *J. Am. Chem. Soc. 101*, 7401–7402.

Chang, C. K., & Dolphin, D. J. (1975) *J. Am. Chem. Soc. 97*, 5948–5950.

Chang, C. K., & Dolphin, D. J. (1976) *Proc. Natl. Acad. Sci. U.S.A. 73*, 3338–3342.

Collman, J. P., & Sorrell, T. N. (1975) *J. Am. Chem. Soc. 97*, 4133–4134.

Collman, J. P., Brauman, J. I., Halbert, T. R., & Suslick, K. S. (1976) *Proc. Natl. Acad. Sci. U.S.A. 73*, 3333–3337.

Dawson, J. H., & Eble, K. S. (1986) *Adv. Inorg. Bioinorg. Mech. 4*, 1–64.

Debrunner, P. G., Gunsalus, I. C., Sligar, S. G., & Wagner, G. C. (1978) in *Metals in Biological Systems* (Siegel, H., Ed.) Vol. 7, pp 241–275, Marcel Dekker, New York.

Garfinkel, D. (1958) *Arch. Biochem. Biophys. 77*, 493–509.

Gelb, M. H., Heimbrook, D. C., Mälkönen, P., & Sligar, S. (1982) *Biochemistry 21*, 370–377.

Groves, J. T., McClusky, G. A., White, R. E., & Coon, M. J. (1978) *Biochem. Biophys. Res. Commun. 81*, 154–160.

Gunsalus, I. C., & Sligar, S. G. (1978) *Adv. Enzymol. Relat. Areas Mol. Biol. 47*, 1–44.

Gunsalus, I. C., Meeks, J. R., Lipscomb, J. D., Debrunner, P. G., & Munck, E. (1974) in *Molecular Mechanisms of Oxygen Activation* (Hayaishi, O., Ed.) Chapter 14, Academic Press, New York.

Hahn, J. E., Hodgson, K. O., Andersson, L. A., & Dawson, J. H. (1982) *J. Biol. Chem. 257*, 10934–10941.

Hanson, L. K., Eaton, W. A., Sligar, S. G., Gunsalus, I. C., Gouterman, M., & Connell, C. R. (1976) *J. Am. Chem. Soc. 98*, 2672–2674.

Heidner, E. J., Ladner, R. C., & Perutz, M. F. (1976) *J. Mol. Biol. 104*, 707–722.

Hendrickson, W. A., & Konnert, J. H. (1980) in *Computing in Crystallography* (Diamond, R., Ramaseshan, S., & Venkatesan, K., Eds.) pp 1301–1323, Indian Institute of Science, Bangalore, India.

Kau, L.-S., Svastits, E. W., Dawson, J. H., & Hodgson, K. O. (1986) *Inorg. Chem. 25*, 4307–4309.

Klingenberg, M. (1958) *Arch. Biochem. Biophys. 75*, 376–386.

Koch, S., Tang, S. C., Holm, R. H., Frankel, R. B., & Ibers, J. A. (1975) *J. Am. Chem. Soc. 97*, 916–918.

Nelson, D. R., & Strobel, H. W. (1988) *J. Biol. Chem. 263*, 6038–6050.

Norvell, J. C., Nunes, A. C., & Schoenborn, B. P. (1975) *Science 190*, 568–570.

O'Keefe, D. H., Ebel, R. E., Peterson, J. A., Maxwell, J. C., & Caughey, W. S. (1978) *Biochemistry 17*, 5845–5852.

Peng, S. M., & Ibers, J. A. (1976) *J. Am. Chem. Soc. 98*, 8032–8036.

Poulos, T. L., & Howard, A. J. (1987) *Biochemistry 26*, 8165–8174.

Poulos, T. L., Perez, M., & Wagner, G. C. (1982) *J. Biol. Chem. 257*, 10427–10429.
Poulos, T. L., Finzel, B. C., Gunsalus, I. C., Wagner, G. C., & Kraut, J. (1985) *J. Biol. Chem. 260*, 16122–16130.
Poulos, T. L., Finzel, B. C., & Howard, A. J. (1986) *Biochemistry 25*, 5314–5322.
Poulos, T. L., Finzel, B. C., & Howard, A. J. (1987) *J. Mol. Biol. 192*, 687–700.
Raag, R., & Poulos, T. L. (1989) *Biochemistry 28*, 917–922.
Shaanan, B. (1983) *J. Mol. Biol. 171*, 31–59.
Steigemann, W., & Weber, E. (1979) *J. Mol. Biol. 127*, 309–338.
Stern, J. O., & Peisach, J. (1974) *J. Biol. Chem. 249*, 7495–7498.
Uno, T., Nihsimura, Y., Makino, R., Iizuka, T., Ishimura, Y., & Tsuboi, M. (1985) *J. Biol. Chem. 260*, 2023–2026.
Wagner, G. C., & Gunsalus, I. C. (1982) in *The Biological Chemistry of Iron* (Dunford, H. B., Dolphin, D., Raymond, K., & Sieker, L., Eds.) pp 405–412, Riedel, Boston.
Wells, A. F. (1986) *Structural Inorganic Chemistry*, Oxford University Press, Oxford.
Yu, C. A., & Gunsalus, I. C. (1974) *J. Biol. Chem. 249*, 102–106.

Crystal Structure of Guanosine-Free Ribonuclease T_1, Complexed with Vanadate(V), Suggests Conformational Change upon Substrate Binding[†,‡]

Dirk Kostrewa, Hui-Woog Choe, Udo Heinemann, and Wolfram Saenger*
Institut für Kristallographie, Takustrasse 6, 1000 Berlin 33, FRG
Received January 25, 1989; Revised Manuscript Received May 1, 1989

ABSTRACT: Ribonuclease T_1 was crystallized in the presence of vanadate(V). The crystal structure was solved by molecular replacement and refined by least-squares methods using stereochemical restraints. The refinement was based on data between 10 and 1.8 Å and converged at a crystallographic R factor of 0.137. Except for the substrate-recognition site the three-dimensional structure of ribonuclease T_1 closely resembles the structure of the enzyme complexed with guanosine 2′-phosphate and its derivatives. A tetrahedral anion was found at the catalytic site and identified as $H_2VO_4^-$. This is the first crystal structure of ribonuclease T_1 determined in the absence of bound substrate analogue. Distinct structural differences between guanosine-free and complexed ribonuclease T_1 are observed at the base-recognition site: The side chains of Tyr45 and Glu46 and the region around Asn98 changed their conformations, and the peptide bond between Asn43 and Asn44 has turned around by 140°. We suggest that the structural differences seen in the crystal structures of free and complexed ribonuclease T_1 are related to conformational adjustments associated with the substrate binding process.

Ribonuclease T_1 (RNase T_1; EC 3.1.27.3) is an endoribonuclease secreted by the fungus *Aspergillus oryzae*. It cleaves RNA highly specifically at the 3′-phosphate group of guanylic acid. The enzyme occurs in two isoforms containing either Gln or Lys at position 25 (Gln25-RNase T_1 or Lys25-RNase T_1). Recently, several crystal structures of RNase T_1–substrate analogue complexes have been determined at high resolution: Gln25-RNase T_1*2′-GMP[1] (Sugio et al., 1985a, 1988), Lys25-RNase T_1*2′-GMP (Arni et al., 1987, 1988), Lys25-RNase T_1*G-(2′–5′)-pG (Koepke et al., 1989), and Gln25-RNase T_1*3′-GMP (Sugio et al., 1985b). However, the tertiary structure of substrate analogue free RNase T_1 was not known so far. Martin et al. (1980) described the crystallization of free RNase T_1, but a structure analysis was not reported. We had intended to cocrystallize RNase T_1 with guanosine–vanadate as a transition-state analogue but instead obtained the RNase T_1–vanadate complex, for reasons explained under Experimental Procedures. We report here the three-dimensional structure of guanosine-free Lys25-RNase T_1 and discuss the conformational differences between substrate analogue free Lys25-RNase T_1 and Lys25-RNase T_1 complexed with 2′-GMP, designated RNase T_1*2′-GMP.

Table I: X-ray Data

space group	$P2_12_12_1$ (No. 19)
lattice constants[a]	
a	48.82 (3) Å
b	46.53 (2) Å
c	41.20 (2) Å
total no. of measured reflections	11 536
$R_{sym} = \sum_h\sum_i\lvert\langle F_h\rangle - F_{h,i}\rvert/\sum_h\sum_i F_{h,i}$	0.029[b]
unique reflections	
$F_o \geq 1\sigma$	7134
$F_o \geq 3\sigma$	6503
completeness of data set at 1.8-Å resolution ($F_o \geq 1\sigma$)	
1.8-Å sphere	0.77
2.0–1.8-Å shell	0.59

[a] Numbers in parentheses are standard deviations and refer to the last digit. [b] Based on 1627 measurements in 804 unique reflections.

Experimental Procedures

Lys25-RNase T_1 was isolated by the method of Fülling and Rüterjans (1978). The guanosine–vanadate was prepared by

[†] This work was supported by the German Federal Minister for Research and Technology (BMFT) under Contract 05 313 IA B3, by the Deutsche Forschungsgemeinschaft through Sonderforschungsbereich 9 (Teilprojekt A7), and by the Fonds der Chemischen Industrie.
[‡] Crystal structure coordinates have been submitted to the Brookhaven Protein Data Bank.

[1] Abbreviations: 2′-GMP, guanosine 2′-phosphate; G-(2′–5′)-pG, guanylyl-(2′–5′)-guanosine; 3′-GMP, guanosine 3′-phosphate; rms, root mean square; Wat, water; MD, molecular dynamics.

0006-2960/89/0428-7592$01.50/0